Stony Brook University

Interfacial Polymerization on Cellulose Nanofiber-Based Membrane as a New Pathway for Fabrication of Thin Film Nanocomposite Membrane

A Thesis Presented

by

ZhiRui Mo

to

The Graduate School

in Partial Fulfillment of the

Requirements

for the Degree of

Master of Science

in

Chemistry

Stony Brook University

August 2012

Stony Brook University

The Graduate School

ZhiRui Mo

We, the thesis committee for the above candidate for the

Master of Science degree, hereby recommend

acceptance of this thesis.

Benjamin Chu– Thesis Advisor
Distinguished Professor
Department of Chemistry

Benjamin S. Hsiao–Thesis Advisor
Professor and Chair
Department of Chemistry

Peter Khalifah – Chair
Professor
Department of Chemistry

Andreas Mayr– Third member
Professor
Department of Chemistry

This thesis is accepted by the Graduate School

Charles Taber
Interim Dean of the Graduate School

Abstract of the Thesis

Interfacial Polymerization on Cellulose Nanofiber-Based Membrane as a New Pathway for Fabrication of Thin Film Nanocomposite Membrane

by

ZhiRui Mo

Master of Science

in

Chemistry

Stony Brook University

2012

Conventional thin film nanocomposite (TFNC) membranes are based on porous membranes produced by the phase inversion method. The top barrier layer in these membranes has smaller pores with a torturous pathway and together with fairly low porosity for the supporting layer, resulting in a relatively low flux. In this study, a high flux ultra-filtration cellulose nanofiber-based (CN) membrane which consists of a three-tier composite structure, consisting of a TEMPO-oxidized cellulose nanofiber top layer, an electrospun poly(acrylonitrile) (PAN) scaffold and a non-woven polyethylene terephthalate (PET) support was used as a substrate for the thin film nanocomposite membrane preparation. The properties of the cellulose nanofiber-based membrane were fully characterized. The barrier layer of this membrane was prepared by interfacial polymerization (IP) of m-phenylenediamine (MPD) and piperazine (PIP) with trimesoyl chloride (TMC) on top of the CN membrane. The interfacial polymerization between MPD and TMC was investigated by studying the effects of the MPD concentration change,

reaction time and curing temperature. Besides, the addition of PIP into the aqueous phase greatly improves the permeate flux without sacrificing the rejection ratio. When the MPD and PIP concentration were 1.5% and 0.5%, respectively, the thin film nanocomposite membrane with CN substrate exhibited a rejection of 94.6% and a permeate flux of 30.5 L/m^2h, about 2 times higher than that of only 2% MPD concentration. Such thin film nanocomposite membrane has about 30% lower permeate flux than the commercial membrane, Dow FilmtecXLE-440 with a comparable rejection ratio (~95%) due to the thicker barrier layer produced by a manual preparation process. In addition, the *A* and *B* values of this TFNC membrane were 4.3 ± 0.1 L/(m^2•h•bar) and 1.54 L/m^2h, compared with the commercial membrane, Dow filmtec XLE-440, 6.9 L/m^2h•bar and 3.06 L/m^2h, respectively. The filtration performance of this thin film nanocomposite membrane under various applied pressures (100~800 psi) was also studied.

Table of Contents

List of Equations

List of Tables

List of Figures

Acknowledgement

I would like to express my deep gratitude and respect to my research advisors Professor Benjamin Chu and Professor Benjamin S. Hsiao for their invaluable advice, continuous patience, stimulating support and encouragement to my research. They are the ones I would admire and appreciate in all my life. Their strict attitude towards the scientific research deeply impressed me and will greatly influence my future career. I would also like to give my thanks to my committee members, Professor Peter Khalifah and Professor Andreas Mayr for their help, suggestions and their encouragements on my way to the M.S. degree. Special thanks should also be given to the Student Affairs Coordinator of the Chemistry Department – Katherine M. Hughes, who I bothered most in the past two years, for her great help with numerous issues.

Many thanks to our current and previous group members Si Hui Guan, Ran Wang, Xiaowei Li, Xiao Wang, Zhe Wang, Rui Yang, Ying Su, Justin Che, Yang Liu, Tsung Ming Yeh, Drs. Dufei Fang, Hongyang Ma, Shigeyuki Toki. Thank them for their all kinds of help in research or daily life, as well as their helpful discussion in my thesis writing. Finally, I would like to express my special appreciation to my parents and friends for their continuous understanding and support. I am also thankful for everyone that I have had in my life.

1. Introduction

Clean water is essential to human health, agriculture and industry. However, the access to clean water is becoming less available to humans due to the growing global population and increasing pollution. Water scarcity has been a global issue which hinders our future development. In particular, people in developing countries in Africa and Asia are suffering a serious clean water crisis. To tackle this problem, the technology of purifying and recycling municipal, industrial and commercial waste water becomes important. Many different methods and procedures, including chemical treatment, physical treatment, biological treatment, have been adopted to better solve the problem. [1-6]The filtration process is the most promising technology to efficiently obtain purified water due to its relatively low energy cost and simplicity. Based on the pore size of the membrane, it can be classified into four types of filtration, microfiltration (MF), ultrafiltration (UF), nanofiltration (NF) and reverse osmosis (RO), shown as **Figure** 1[7].

Among the different processes, nanofiltration offers the best potential to meet the huge freshwater demand in the future since 97% of earth's water is sea water. It has overtaken conventional thermal technology, such as multi-stage flash distillation (MSF),and has a better promising future than other technologies, such as distillation, electro-dialysis, and capacitive deionization. [8-12]

1.1 Nanofiltration—the leading desalination technology

Nanofiltration is the process of removing dissolved salts and other minerals from seawater and brackish water (*e.g.* river water) to obtain water suitable for human and animal consumption,

irrigation and other industrial uses. [13] It applies high pressure (more than 100 psi) to overcome the osmotic pressure of the salts, allowing water to pass through the semipermeable membrane. The osmotic pressure mainly depends on the salt concentration (particularly NaCl), and higher salt concentration requires higher applied pressure to create water flow. The osmotic pressure (∏) is defined as **Equation** 1.

1.1.1 Separation mechanism of desalination

Generally, nanofiltration membrane is considered to have a barrier layer with very small pores (~0.5 nm diameter). It is known that the Donnan exclusion, the requirement of charge neutrality and solution-diffusion effect all contribute to the mechanism of the salt rejection. [14]For example, when a negatively charged membrane is present, the positively charged ion concentration is higher in the membrane phase than in the bulk solution, and the negatively charged ion concentration is lower in the membrane phase. The uneven electrical charge distribution in the solution is the result of Donnan equilibrium which creates a potential difference at the interphase, called the Donnan potential. The transport of negatively charged ions in the membrane phase does not favor the Donnan equilibrium, resulting in a repulsion of negatively charged ions from the membrane. [15] The positively charged ions are also rejected because of the electro-neutrality requirement. A schematic diagram of the Donnan effect on a negatively charged membrane is shown in **Figure**2.

The ideal nanofiltration membrane which has a very dense structure is not suitable for convective transport. Salt transport may take place by solution-diffusion instead of convective transport. Due to the higher diffusivity of NaCl than that of other salts (such as Na_2SO_4, $MgSO_4$), the rejection of NaCl would be lower than those of other salts. Generally, the solution-diffusion transport is dominant in the nanoflitration system.

1.1.2 Transport properties of desalination membrane

According to the solution-diffusion mechanism, water and salt ions can molecularly diffuse through the membrane material as a consequence of a concentration gradient. [16] The passages of water and salt ions through the membrane are expressed as the water and salt flux. They can be described by mathematical modeling of the concentration profiles of the membrane. The water flux (pure water permeability) J_w is given as **Equation** 2.Theoretically, it is the intrinsic property of the nanofiltration membrane regardless of the pressure. The salt flux through the membrane J_S, is given as **Equation** 3.[17] Conventionally, the transport properties of the nanofiltration membranes are reported as water and salt permeability in terms of *A, B* values. The formulas of the *A, B* values are given as **Equation** 4 and **Equation** 5, respectively.[18]

1.2 Novel high-flux cellulose nanofiber-based membrane as nanofiltration membrane substrate

According to different chemical compositions and structures, the membranes could be classified as isotropic and anisotropic or symmetric and asymmetric. The word “anisotropic” or “asymmetric” means that the membranes are non-uniform over the membrane cross-section, and they usually consist of layers which vary in structure and chemical composition. Conventionally, in the nanofiltration membrane preparation, the interfacial polymerization is performed on top of an asymmetric ultrafiltration membrane. This substrate is usually prepared by the phase inversion method which casts a polysulfone (PS) or polyethersulfone (PES) solution on top of the substrate. The cross-section SEM image of a typical PS membrane is shown as **Figure** 3 [19], showing that the PS membrane has a thin and dense barrier layer supported by a finger-like microporous structure.

However, such structures have certain limits. For example, the pores in the microporous layer are not interconnected, resulting in a lower porosity with more limited flux. The hydrophobic barrier layer is also subject to the fouling issue.

In this study, a novel cellulose nanofiber-based membrane which is a thin-film nanofibrous composites (TFNC) ultrafiltration membrane is used as the thin film nanocomposite membrane substrate. It consists of a three-layer structure, as shown in **Figure** 4.

The unique features of high-flux cellulose nanofiber (CN) membranes for water purification (*e.g.* bilge water cleaning through ultrafiltration (UF)) have recently been demonstrated by Hongyang Ma et al. [20]. The breakthrough performance of the cellulose nanofiber-based ultrafiltration membrane is that the top CN layer is a very thin (several hundred nanometers thickness)and strong as well as it can be functionalized. This barrier layer is formed by deposition of very fine cellulose nanofibers (diameters in the 5–10 nm range as determined by TEM). The modified cellulose nanofibers obtained by using the TEMPO oxidation method can create a hydrophilic and fairly smooth surface for the interfacial polymerization (contact angle 10.9^{o}). [21, 22]The mid-layer consists of a polyacrylnitrile (PAN) nanofibrous scaffold (with fiber diameters in the hundreds of nanometers) fabricated by electro-spinning, being different from a conventional asymmetric membrane, produced by the phase inversion process. Both the CN layer and the electrospun PAN scaffold has a high porosity (~80% or more) and the pores are highly interconnected, creating a high flux support for the nanofiltration barrier layer. The bottom part is non-woven material, polyethylene terephthalate (PET), providing a good mechanical strength for the top layers. The crucial advantages of the UF cellulose fibrous membrane are not only to create a high performance thin film nanocomposite membrane but also

the lower cost of natural materials (such as cellulose) and the simpler preparation procedures related to the cellulose nanofiber formation, which can be adopted for mass production.

1.3 Materials and methods in desalination membrane

1.3.1 Development of conventional desalination membranes

The first desalination membrane was the asymmetric Loeb-Sourirajan membrane using cellulose acetate (CA) which has a dense and thin layer over a micro-porous support in 1960s. It achieved 98% rejection, but a low permeate flux (< 10 L/m^2h) [23]. However, the CA membrane can only be stable in a narrow pH range. In 1970s, the development of interfacial polymerization to produce desalination membranes by Cadotte was a major technological milestone in the history of desalination processes. [24] The invention of NS-100, polyethylenimine reacted with toluene di-isocyanate was the first non-cellulosic membrane with comparable filtration performance to the CA membrane and good stability in high temperature, acidic and alkaline environments. [25, 26]With the use of interfacial polymerization in the desalination process, researchers have spent a great deal of efforts on improving the filtration performance by using different monomers, such as aliphatic amines and terephthaloyl chloride. In 1980s, Cadotte discovered that by using monomeric aromatic amines and aromatic acyl halides, membranes can be produced with greatly improved filtration performance. The Dow Filmtec FT-30 commercial membrane prepared by m-phenylenediamine (MPD) and trimesoyl chloride (TMC) became a success and had a significant impact on the design and cost of desalination.[27] In the past twenty years, barrier layer modification, such as post treatment and hydrophilization, has been extensively investigated to improve permeate flux, rejection ratio, chloride stability and fouling resistance. In addition,

inorganic materials(*i.e.*, zeolite, carbon nanotube, TiO_2) have been used as additives to modify the barrier layer of desalination membranes. [28]

1.3.2 Polyamide barrier layer prepared by interfacial polymerization with additive of piperazine (PIP)

Interfacial polymerization technology has been widely used in desalination membrane preparation since 1970s. Especially, the success of Dow Filmtec FT-30 with the use of MPD and TMC significantly impacts the desalination development. Interfacial polymerization produces ultrathin films at the interface between two immiscible phases upon contact. Generally, amine monomers are in the aqueous phase and acyl halides are in the organic phase. The reaction takes place very fast (less than 1 second) [29] and continued polymerization leads to the formation of a dense layer that hinders diffusion of amine across the film, resulting a very thin film (~several hundred nanometer thickness). In the present study, trimesoyl chloride was chosen as the aromatic acyl halide. It has three chloride groups and is able to form a 3D crosslinked polyamide network. M-phenylenediamine and piperazine were chosen as the aromatic amines. The addition of PIP in the aqueous phase avoids the excessively tight crosslinking and low free volume of the barrier layer which lower the water permeability. A schematic diagram of the formation of polyamide barrier layer by interfacial polymerization is shownin**Figure**5.

The membrane substrate was saturated with MPD and PIP aqueous solution and then covered by the organic phase with TMC. A dense polymer network was formed with crosslinking between MPD, PIP and TMC by peptide bonds (-C(O)NH-). During the reaction, TMC was partially hydrolyzed by contacting with water, forming the carboxylic group (-

COOH). Since MPD and PIP had better solubility in the organic phase than that of TMC in the aqueous phase, the reaction zone was shifted deeper within the organic phase as the reaction was progressed. The forming film would be located in the organic phase.

In this study, the cellulose nanofiber-based membrane was used as a thin film nanocomposite membrane substrate for the barrier layer fabricated by means of interfacial polymerization. The monomeric amine, MPD and PIP, and aromatic acyl halide, TMC were used to prepare the thin film nanocomposite membrane barrier layer via IP. The effects of amine concentrations, reaction time and curing temperature on the filtration performance were investigated to improve the permeate flux without sacrificing the rejection ratio.

2. Materials and Methods

2.1 Materials

Non-woven poly(ethylene terephathalate) (PET) substrate (PET microfilter AWA#16 with an average fiber diameter of about 19 μm) for membrane support was provided by Sanko (Japan). Polyacrylonitrile（PAN）with a weight average molecular weight of 1.5 x 10^5 g/mol was purchased from Polyscience, Inc. Dimethylformamide (DMF) from Sigma-Aldrich was used as a solvent for PAN. Cellulose Biofloc 96 (wood bleached pulp) was provided from the Tembec factory in France. Cotton linter pulps, ER10 (DP_w 1320) and UVE (DP_w 7350), were supplied by Buckeye Technologies, Inc in USA. 2,2,6,6-tetramethyl-1-piperidinyloxy (TEMPO), sodium hypochlorite (NaClO) solution (available chlorine 10~15%) and sodium bromide (NaBr) from Sigma-Aldrich were used for cellulose modifications. Piperazine (PIP), m-phenylenediamine

(MPD) and trimesoyl chloride (TMC) were purchased from Sigma-Aldrich for the interfacial polymerization.

2.2 Preparation of cellulose nanofiber-based ultrafiltration membrane

2.2.1 Preparation of electrospun PAN substrate

PAN was dissolved in DMF at 60 °C for 2 days until it became a homogeneous solution (solution concentration 10 wt%). The PAN solution was electrospun onto non-woven PET support at 20 kV. The flow rate was 16 μl/min and spinneret diameter was 0.7 mm. The working distance between the collector and the spinneret was 10 cm. The mean fiber diameter was 220 ± 10 nm and the maximum pore size from bubble point test was 0.78 μm.

2.2.2 Preparation of cellulose nanofibers and cellulose barrier layer

The cellulose nanofiber preparation was fully described in the literature.[21] Cellulose dry sample (2 g) was dispersed in water (192 g). Sodium bromide (0.20 g) and TEMPO (0.04 g) were dissolved in the same suspension. The reaction was started by adding sodium hypochlorite solution (30.0 g, 10–13 % aqueous solution) with use of a medicine dropper at an estimated speed of 15g per minute under a stirring speed of 500 rpm and it lasted for24 h. The pH value was kept at 10.0–10.3, monitored with a pH meter and adjusted by using a sodium hydroxide aqueous solution (0.5 mol/L). The reaction was stopped by adding ethanol (10 mL), followed by stirring for 20 min. The final product was separated by centrifuging the reaction mixture (5000 rpm), followed by washing with DI water 5 times and then separating again by centrifugation. The oxidized cellulose microfiber slurry was kept in a refrigerator. Oxidized cellulose

microfibers (0.05 g) [or oxidized cellulose slurry (1.10 g)] were dispersed in 100 g of water and sonicated for 5 min with a homogenizer (Cole Parmer, VCX-400). The suspension was centrifuged at 5000 rpm, and the recovered supernatant became the cellulose nanofiber aqueous suspension with a concentration of ~ 0.05 wt %.

The cellulose nanofiber coating procedure has been described elsewhere [21]. Briefly, the electrospun PAN nanofibrous scaffold/PET nonwoven support was immersed in water (pH = 1.5). The cellulose nanofiber aqueous suspension (0.05 wt%, pH = 4) was then cast on top of the support. The barrier layer thickness was controlled by the gap of a coating knife. After coating, the cellulose nanofiber membrane was dried at 70 ^{o}C for 20 min.

2.3 Preparation of polyamide thin film nanofibrous composites (TFNC) membrane

A CN UF membrane was immersed in an aqueous solution of MPD and PIP for 2 minutes and the membrane was rolled with a soft rubber roller to remove excess solution. The MPD/PIP-saturated CN membrane was then covered with a solution of 0.1% (w/v) TMC in hexane for various times (5 to 60 seconds). The excess TMC solution was drained, and the membrane was dried in an oven at 70^{o}C for 15 minutes. [19]

2.4 Membrane characterization methods

2.4.1 Scanning electron microscopy (SEM)

The morphology of membrane was detected by SEM (Phenom^{TM} from FEI, Inc). All specimens received one minute of gold coating. The cross-sectioned samples were prepared by

fracturing water-wetted membrane in liquid nitrogen. The fiber diameters, fiber diameter distributions and cellulose nanofiber barrier layer thickness were determined by using the SEM images together with a modified LeiKa software developed at Stony Brook (www.dell.chem.sunysb.edu).

2.4.2 Pore size determination of electrospun PAN scaffold

A capillary flow porometer (CFP-1500A from PMI porous material, Inc) was used to determine the pore size of electrospun PAN scaffold. The Galwick wetting fluid was used for the bubble point test.

2.4.3 Molecular weight cut-off (MWCO) test

A series of dextrans (form Leuconstocmesenteroides, Sigma) with different molecular weights: 4-6 KDa, 9-11 KDa, 15-17 KDa, 35-45 KDa, 64-76 KDa, 100-200 KDa, 200-300 KDa, 425-575 KDa, 2000 KDa and 5000 KDa, were dissolved in Milli-Q water to prepare 5000 ppm of feed solutions in the presence of sodium azide (500 ppm). The solutions were used to test the molecular weight cut-off (MWCO) of the cellulose nanofibrous membrane. The applied pressure was 10 psi and the temperature was 25^{o}C. A total organic carbon analyzer (TOC-5000, Shimazu Corp) was applied to determine the results of MWCO.

2.4.4 Desalination membrane performance test

Membrane filtration performance was evaluated by using a lab-made cross-flow system. The test was operated at room temperature (25 ^{o}C) for 6 hours. All the measurements were collected

after a 3-hour operation. The feed solution was 500 ppm NaCl aqueous solution, and its pH value was controlled at 8. The applied pressure and flow rate were 100~800 psi and 1 gallon per minute (GPM), respectively. The water permeability and the salt rejection were measured after a 3-hour operation. The rejection ratio(*R*) was calculated as **Equation** 6. The salt concentrations were measured by using a conductivity meter. The permeate flux can reflect permeability of the membrane, which is defined as volume per unit area per unit time and is shown as **Equation** 7.

3. Results and Discussions

3.1 Properties of cellulose nanofiber membrane

The properties of electrospun PAN nanofibrous scaffold, PET non-woven substrate and cellulose nanofiber barrier layer are listed in **Table** 1.

3.1.1 Properties of electrospun PAN nanofibrous scaffold and PET non-woven support

The PET non-woven membrane was chosen as the support of the TFNC cellulose nanofiber membrane. Its mechanical properties were determined by the previous study[20], showing that it was the main load bearing component, responsible for the mechanical strength. [20] The average thickness of PET support and electrospun PAN scaffoldwere104.4 ± 1.7 μm and 37.3 ± 6.4 μm (determined by the use of micrometer), respectively. A SEM image of the top view of the PET non-woven support and fiber diameter distribution are shown in **Figure** 6.

The PET support had an average fiber diameter of $(1.9\pm 0.9)\times 10^4$nm which was about 100 times larger than that of the electrospun PAN scaffold (220 ± 50 nm), as determined in **Figure**7 and **Figure** 8.

The average fiber diameter of electrospun PAN scaffold from the top view and side view were in good agreement which was different by only 10 nm. The mean and the maximum pore size of PAN nanofibrous scaffold were determined to be 0.65 ± 0.1 μm and 0.78 ± 0.1 μm by using the porometer. The pore size distribution is shown as **Figure** 9.

3.1.2 Characterization of functional groups of cellulose nanofibers

Different cellulose sources, wood pulp and cotton linter pulps, were treated with two TEMPO oxidation conditions (5.4 and 8.7 mmol NaClO/g cellulose sample). With increasing amounts of NaClO, the degree of TEMPO oxidation for the cellulose nanofiber would be higher. After the TEMPO oxidation, the oxidized cellulose nanofibers usually had carboxylate groups and aldehyde groups. The functional group contents (carboxylate group –COOH and aldehyde group –CHO) were determined based on the electric conductivity titration method [30,31] and summarized in **Table** 2.

With higher amounts of carboxylate groups(~1 mmol/g cellulose) in the cellulose nanofibers, the materials should become more hydrophilic. Such cellulose nanofibers could be suspended in water with little aggregation. The aldehyde group was the intermediate during the oxidation of C6 hydroxyl group to the carboxylate group. The presence of the aldehyde group could be used to create thermal crosslinking during the drying process, and thereby improving the mechanical

strength of the cellulose nanofiber barrier layer. The thermal crosslinking reaction between the C6 hydroxyl group and the aldehyde group is illustrated in **Figure** 10.

In Table 2, with increasing amounts of NaClO, the carboxylate group content of each cellulose source was increased from ~1 mmol/g to 1.5~1.8 mmol/g cellulose. Only the Biofloc 96 at 5.4 mmol NaClO/g cellulose had aldehyde groups of ~0.34 mmol/g cellulose which could provide higher mechanical stability for the cellulose nanofiber barrier layer via significant thermal crosslinking.

3.1.3 Properties of cellulose nanofiber barrier layer

. The cellulose nanofibers from different cellulose sources which were prepared under the same TEMPO oxidation condition (5.4 mmol NaClO/g cellulose) was used to fabricate cellulose nanofiber barrier layers, being coating on electrospun PAN scaffold. The corresponding cellulose nanofiber UF membranes were tested in the filtration performance test. From **Table** 3, cellulose nanofiber membrane based on Biofloc 96 has at least 10% higher pure water flux than those based on other two cotton linters. The rejection ratio of 2000K Dextran of Biofloc 96 was significantly (30%) higher than those of cotton linter. The reason could be cellulose nanofiber of Biofloc 96 had a shorter fiber length than that of cotton linters. Shorter fiber length could allow cellulose nanofibers to stack much tighter, resulting in a higher density in the cellulose nanofiber barrier layer. It could produce smaller pore size in the membrane surface. Therefore, CN membrane of Biofloc 96 could reject more 2000K Dextran than those of cotton linters. The UF membrane of Biofloc 96 provided a better substrate for the desalination membrane preparation.

The cellulose nanofiber UF membrane based on Biofloc 96 was further investigated. SEM measurements were carried out to investigate the thickness of the cellulose barrier layer as well as the surface morphology. **Figure** 11 shows the top and cross-section views of the cellulose nanofiber layer.

The cellulose nanofiber forms a uniform and integrated thin film on top of the PAN nanofibrous scaffold. From the cross-section view, the PAN electrospun nanofibers were imbedded in the cellulose barrier layer, and the integrated nanocomposite format reinforced the mechanical strength of the barrier layer. [20] The barrier layer thickness was determined to be 240 ± 30 nm from the cross-sectional SEM image.

The MWCO property of the cellulose nanofiber membrane was evaluated using aqueous dextran solutions over a range of different molecular weights. The average pore size of the tested membrane could be estimated by using the Stokes-Einstein radius (r_s in Å) based on the following empirical equation (**Equation** 8).[32]

According to the TOC result, the cellulose nanofiber membrane had 90.8 % rejection ratio of 5000 KDa dextran which corresponded to a molecule diameter of 83.4 nm (the pore size $d_p = 2r_s$), indicating a maximum pore size of about 83.4 nm. The pore size distribution of the membrane could be determined by using a series MWCO tests with dextran, and is shown in **Figure** 12. [33, 34, 35]

3.2 Filtration performance of thin film nanocomposite membrane produced by interfacial polymerization with MPD and TMC

3.2.1 The effect of concentration of m-phenylenediamine (MPD) on filtration performance

The filtration performance data were collected after a 3-hour operation. The permeate flux and the salt rejection were more sensitive to changes in the MPD concentration than the TMC concentration due to the fact that the IP reaction was mainly controlled by the diffusion of MPD through the interfacial polymerized film since the reaction occurred in the organic phase. In the present study, the MPD concentration varied from 1 % to 4% and its effect on the filtration performance was investigated. From **Figure** 13, the permeate flux decreased from 9.0 to 8.1L/m^2h and the rejection increases from 91% to96% when the MPD concentration was increased from 1% to 2.5%. As the MPD concentration was increased, it had a higher diffusivity into the organic phase. [34]

As a result, higher MPD concentration would be in the organic phase and created a higher crosslinked polyamide network, resulting in a tighter and thicker IP thin film at the interface. On the other hand, TMC would hydrolyze when in contact with water before reacting with MPD at low MPD concentration, and a relatively loose polyamide network was formed. Therefore, the rejection would be low (such as 91.2% at 1% MPD concentration). However, as the MPD concentration was increased from 2.5% to 4%, too many MPD monomers could be present in the organic phase, and both amine groups in the MPD monomer was not able to react with the acyl halide groups in TMC since TMC was the limiting reagent. An integrated polyamide network could be formed, and the loose network resulted in having the polyamide thin film with larger

pore sizes. Therefore, the rejection ratio was decreased and the permeate flux was increased. The results suggested that the optimum MPD concentration was 3%, yielding a permeate flux of 10.7 L/m^2h with a rejection rate of 96.6%.

3.2.2 The effect of reaction time on filtration performance

The effect of reaction time on filtration performance was investigated. MPD and TMC concentrations were 3% and 0.1% w/v, respectively. The reaction time was changed from 5 to 60s. From **Figure** 14, the rejection ratio and the permeate flux changed by only ~0.3% and ~10%, respectively.

It is implied that the growth of the polyamide thin film stopped after a 5-second reaction time since the quick formation of the polyamide thin film would hinder the movement of MPD monomers into the organic phase. It has been suggested that the polyamide thin film via interfacial polymerization is formed in less than a second. A novel coating method (such as slot die) which can reduce the reaction time is preferred to produce a much thinner barrier layer, and it could improve the filtration performance.

3.2.3 The effect of curing temperature change on filtration performance

Heat curing is often required to facilitate the removal of residual organic solvent from nascent polyamide thin films and to promote additional crosslinking by dehydration of unreacted amine and carboxyl groups. The curing temperature was changed from 55 to 95 ^oC. From **Figure** 15, when the curing temperature was 55^oC, the permeate flux was improved to 12.1 L/m^2h, which was 20% higher than that at 95^oC. The rejection ratio remained at 96.6%, suggesting that

lowering the curing temperature could prevent excess further crosslinking during the drying stage.

3.3 Filtration performance of thin film nanocomposite membrane with addition of PIP in aqueous phase

3.3.1 Addition of PIP at 3 wt% m-phenylenediamine (MPD)

From section 3.2.1, 3% MPD concentration could exhibit a good filtration performance. However, its permeate flux was only 10.7 L/m^{2}h which was much lower when compared with the commercial membrane Dow Filmtec XLE-440 with a permeate flux of 48.4 L/m^{2}h. In order to further increase the permeate flux, PIP was added into the aqueous phase with MPD. Generally, the reaction between MPD and TMC would create a polyamide network with hydrogen bondings since MPD was the primary amine. PIP was the secondary amine with only one hydrogen connected to the nitrogen atom. A hydrogen atom was lost after the interfacial polymerization. The involvement of PIP in the interfacial polymerization reduced hydrogen bondings in the polyamide network, resulting in a network with more free volume. More free volume in the polyamide network could introduce more pathways for water molecules to pass through the membrane with lower restrictions for water passage through the membrane, and thereby improving the water flux. The effect of different PIP concentrations from 0.3% to 2% on the filtration performance was examined. From **Figure** 16, the permeate flux for 0.3%, 0.6% and 2% were 19.3, 21.6 and 18.6 L/m^{2}h, respectively. It was at least 80% higher than that of only 3% MPD in the aqueous phase. When the PIP concentration was 2%, the total amine concentration was 5%. With a thicker film, the water flux was decreased. The rejection ratio for the whole PIP

concentration range remained above 95.3%, which was only ~1% lower than that of only 3% MPD in the aqueous phase. The 0.6% PIP concentration hada permeate flux of 21.6 L/m^{2}h with a rejection ratio of 95.3 %.

3.3.2 MPD concentration change at 0.5 wt% piperazine (PIP)

From the study of section 3.3.1, it is found out that high total amine concentration could produce a high diffusivity in the organic phase but it increased the thin film thickness and lowered the permeate flux. On the other hand, a low total amine concentration would result in a low rejection ratio due to the loose polyamide network. In order to obtain a higher water flux without sacrificing the rejection ratio, the MPD concentration was varied to optimize the filtration performance, and the PIP concentration was fixed at 0.5 wt%. From **Figure** 17, when the MPD concentration was changed from 0.5% to 3%, the permeate flux decreased from 30.0 to 21.3 L/m^{2}h because of the increasing thin film thickness.

The rejection ratio increased from 91% to 95.5% due to the formation of a tighter polyamide network. In this work, the optimized MPD concentration was 1.5% with a permeate flux of 30.5 L/m^{2}h and a rejection ratio of 94.6 %. Its total amine concentration was 2%, with a flux of about 2 times higher than that of 2% MPD with 95.5 % rejection ratio. The *A* and *B* values of 1.5% MPD concentration were 4.3 ± 0.1 L/m^{2}h•bar and 1.54 L/m^{2}h, compared with the commercial membrane, Dow filmtec XLE-440, 6.9 L/m^{2}h•bar and 3.06 L/m^{2}h, respectively. The lower permeate flux of this thin film nanocomposite (TFNC) membrane is caused by the thicker barrier layer when compared with that of Dow filmtec XLE-440. From **Figure** 18, the barrier thickness of the TFNC membrane and Dow filmtec XLE-440 were estimated to be 260 ± 40 nm and 120 ±

20 nm, respectively. The thickness of the TFNC membrane is around two times higher than that of XLE-440, which is due to the manual interfacial polymerization coating process. Manual coating process could not finely control the barrier layer thickness, resulting in higher restriction for water to pass through the membrane.

The filtration performance of this desalination membrane based on CN membrane substrate was tested under various pressures(100~800 psi) to study the potential application of CN UF membrane substrate under higher pressure conditions. From **Figure** 18, the permeate flux increased almost linearly from 23 to 124 L/m^{2}h with increasing pressure. The normalized permeate flux remained at around 2.6 ± 0.6 L/m^{2}h•bar through the whole pressure range. It should be noted that the osmotic pressure remained the same under various pressures since the salt concentration stayed the same. Therefore, the permeate flux should be mainly dependent on the applied pressure. In addition, the rejection ratio still remained above 95% over the whole pressure range, indicating no leaking had occurred even under fairly high pressures. Thus, the CN UF membrane substrate should have the potential of being used under high pressures (*e.g.* 800 psi) and high salt concentration (*e.g.* 32000 ppm NaCl) conditions.

4. Conclusions

The cellulose nanofiber membrane has a hydrophilic barrier layer with a thickness of about 240 ± 30 nm. From the MWCO test of dextran, the maximum pore size of the cellulose nanofiber membrane is about 83 nm. The study of interfacial polymerization between MPD and TMC showed an optimized MPD concentration of 3%, yielding a permeate flux of 10.7 L/m^{2}h and a rejection ratio of 96.6%. A change in the reaction time from 5 to 60s did not significantly affect

the filtration performance, while the low curing temperature could prevent excess further crosslinking of the polyamide network, and thereby improving the permeate flux. The addition of 0.6% PIP into 3% MPD in the aqueous phase could create more free volume in the polyamide thin film and greatly improved the water flux from 10.7 to 21.6 L/m^{2}h with the rejection ratio remaining above 95%. Optimizing the MPD concentration could further increase the permeate flux without sacrificing the rejection ratio. In this work, the optimized MPD concentration was 1.5% with 0.5% PIP, which had a permeate flux of 30.5 L/m^{2}h with a rejection of 94.6%, 2 times higher than that of only 2% MPD with a 95.5 % rejection ratio. The *A* and *B* values of 1.5% MPD and 0.5%PIP were 4.3 ± 0.1 L/(m^2•h•bar) and 1.54 L/m^{2}h, compared with the commercial membrane, Dow filmtec XLE-440, 6.9 L/m^{2}h•bar and 3.06 L/m^{2}h, respectively. The lower permeate flux of this thin film nanocomposite (TFNC) membrane is due to the thicker barrier layer of 260 ± 40 nm when compared with that of Dow XLE-440, 120 ± 20 nm. The higher thickness of TFNC membrane barrier layer is caused by the manual interfacial polymerization process which could not finely control the barrier layer thickness.

List of Reference

[1] D. Swmi,D. Buddhi. Removal of contaminants from industrial wastewater through various non-conventional technologies: A review, *International Journal of Environment and Pollution*, **2006**, 27(4): 324-346.

[2] M. Cotman, Slovenia, J.Zagorc-Koncan ,A.Drolc, Study of impacts of treated wastewater to the Krka river. *Water Science & Technology*. **2001**, 44(6): 47-54.

[3] A. Dabrowski., Z. Hubicki., P. Podkoscielny, et al. Selective removal of the heavy metal ions from waters and industrial wastewaters by ion-exchange method. *Chemosphere*.**2004**, 56(7): 91-106.

[4] P. Taylor .Removal of trace concentrations of heavy metals using complexing ion-exchange resins. *Separation Science and Technology*.**2006**, 41(8): 2575-2579

[5] D.I. Waqner, C.H. Von, Y, Li, et al. Removal of mercury from chemical wastewater by microorganisms in technical scale. *Environmental Science and Technology*.**2000**, 34(11): 4628-4634

[6] L.Diel.,A.Rynqaert., H.Wouters.,et al. Heavy metals removal by sand filters inoculated with metal sorbing and precipitating bacteria. *Hydrometallurgy*.**2003**, 71(10): 235-241

[7]R.H.Perry, D.W. Green,. Perry's Chemical Engineers' Handbook, 7th ed.; McGraw-Hill: New York, 1997.

[8] Energy Makes All the Difference: Desalination Operating Costs Compared - Chart, *Global Water Intelligence*, 8 (**2007**).

[9] S.T. Hsu, K.T. Cheng, J.S. Chiou, Seawater desalination by direct contact membrane distillation, *Desalination* 143 (**2002**) 279–287.

[10] M. Sadrzadeh, T. Mohammadi, Sea water desalination using electrodialysis, *Desalination* 221 (**2008**) 440–447.

[11] Y. Oren, Capacitive deionization (Cdi) for desalination and water treatment – past, present and future (a Review), *Desalination* 228 (**2008**) 10–29.

[12] R.L. McGinnis, M. Elimelech, Energy requirements of ammonia-carbon dioxide forward osmosis desalination, *Desalination* 207 (**2007**) 370–382.

[13] M. G.Marcovecchio, S. F. Mussati, P. A. Aguirre and N. J. Scenna, Optimization of hybrid desalination processes including multi stage flash and reverse osmosis systems, *Desalination*, **2005**, 182, 111–122.

[14]Alicja M. Mika, James M. Dickson, Pore-filled Membranes Capable of Selective Negative Rejections, *Nature and Science,*2003;1(1):21-26

[15] Bart Van der Bruggen, Carlo Vandecasteele, Dirk Wilms, Influence of ion size and charge in nanofiltration, *Separation and Purification Technology* 14 (**1998**) 155–162

[16]D.R. Paul, Reformulation of the solution-diffusion theory of reverse osmosis, *Journal of Membrane Science* 241 (**2004**) 371–386

[17] Alyson C. Sagle, Benny D. Freeman, James E. McGrath, Water permeability and water/salt selectivity tradeoff in polymers for desalination, *Journal of Membrane Science*369 (**2011**) 130–138

[18] Tzahi Y. Cath, Amy E. Childress, Menachem Elimelech, Forward osmosis: Principles, applications, and recent developments, *Journal of Membrane Science* 281 (**2006**) 70–87

[19] Huanlin Chen, Congjie Gao, Preparation of Reverse Osmosis Composite Membrane with High Flux by Interfacial Polymerization of MPD and TMC , *Journal of Applied Polymer Science*,Vol. 112, 2066–2072 (**2009**)

[20] H.Ma, K.Yoon. et al. High-flux thin-film nanofibrous composite ultrafiltration membranes containing cellulose barrier layer. *J. Mater. Chem*., **2010**, 20, 4692–4704

[21] Hongyang Ma, Christian Burger, Benjamin S. Hsiao,* and Benjamin Chu, Ultrafine Polysaccharide Nanofibrous Membranes for Water Purification, *Biomacromolecules***2011**, 12, 970–976

[22] Yoshiharu Nishiyama, and Akira Isogai, Cellulose Nanofibers Prepared by TEMPO-Mediated Oxidation of Native Cellulose, Biomacromolecules2007, 8, *2485-2491*

[23] Robert J. Petersen, Composite reverse osmosis and nanofiltration membranes, *Journal of Membrane Science, 83* (**1993**) 81-150

[24] KahPeng Lee, Tom C. Arnot, Davide Mattia, A review of reverse osmosis membrane materials for desalination—Development to date and future potential, *Journal of Membrane Science* 370 (**2011**) 1–22

[25] C.R. Bartels, A surface science investigation of composite membranes, *J. Membr. Sci*. 45 (**1989**) 225–245.

[26] K.J. Mysels, W. Wrasidlo, Strength of interfacial polymerization films, *Langmuir* 7 (**1991**) 3052–3053.

[27] F. Crowdus, System economic advantages of a low pressure, spiral RO system using thin composite membranes, *Ultrapure Water* 1 (**1984**) 29.

[28] Dan Li, Huanting Wang, Recent developments in reverse osmosis desalination membranes, *J. Mater. Chem*., **2010**, 20, 4551–4566

[29] Rachel Oizerovich-Honig, Vladimir Raim, and Simcha Srebnik, Simulation of Thin Film Membranes Formed by Interfacial Polymerization, *Langmuir***2010**, 26(1), 299–306

[30] Araki, J.; Wada, M.; Kuga, S. Steric Stabilization of a Cellulose Microcrystal Suspension by Poly(ethylene glycol) Grafting, *Langmuir* 2001, *17*, 21.

[31] Parks, E. J.; Hebert, R. L. *Tappi J.* **1972**, *55* (10), 1510.

[32] D. Venturoli and B. Rippe, Ficoll and dextran vs. globular proteins as probes for testing glomerular permselectivity: effects of molecular size, shape, charge, and deformability, *Am. J. Physiol.: Renal Physiol.*, **2004**, 288, F605–F613.

[33]Kenneth S. McGuire, Kevin W. Lawson, Douglas R. Lloyd, Pore size distribution determination from liquid permeation through microporous membranes, *Journal of membrane science* 99 (**1995**) 127-137

[34]Dapeng Li, Margaret W. Frey, Yong L. Joo, Characterization of nanofibrous membranes with capillary flow porometry, *Journal of Membrane Science* 286 (**2006**) 104–114

[35] A. Hernández, A. Bottino, G. Capannelli, Characterization of UF membranes by liquid–liquid displacement porosimetry, *Desalination* 245 (**2009**) 546–553

Appendices

Equation 1

$$\prod = MRT \quad (1)$$

where M is the concentration of the salts, R is the gas constant (0.08206 L•atm•mol^{-1}•K^{-1}), T is the absolute temperature.

Equation 2

$$\boldsymbol{J_W = A(\Delta P - \Delta \pi)} \quad (2)$$

where A is called the water permeability constant. ΔP and $\Delta\pi$ are the differences in hydrostatic pressure and osmotic pressure across the membrane, respectively.

Equation 3

$$J_S = B \cdot \Delta C_S \quad (3)$$

where B is the salt permeability constant which is independent of pressure. ΔC_S is the salt concentration difference across the membrane.

Equation 4

$$A = \frac{J_W}{(\Delta P - \Delta \pi)} \quad (4)$$

where J_w is the water flux, ΔP and $\Delta\pi$ are the differences in hydrostatic pressure and osmotic pressure across the membrane, respectively.

Equation 5

$$B = \frac{(1\text{-}R)\bullet A\bullet(\Delta P\text{-}\Delta\pi)}{R} \quad (5)$$

where *R* is the salt rejection rate.Δ*P* and Δπ are the differences in hydrostatic pressure and osmotic pressure across the membrane, respectively. *A* is the water permeability constant.

Equation 6

$$R\,(\%) = 100\% \times (1 - C_p/C_f) \quad (6)$$

where C_p and C_f were the salt concentrations of permeate and feed, respectively.

Equation 7

$$P = \frac{\Delta V}{S\cdot\Delta t} \quad (7)$$

where Δ*V* is the permeate volume accumulated during a time interval Δ*t*, *S* is the surface area of the membrane.

Equation 8

$$r_s = 0.33 \times (MW)^{0.463} \quad (8)$$

where *MW* is the molecular weight of dextran in Da.

	Thickness (μm)	Fiber diameter (nm)	Maximum pore size (μm)	Porosity (%)	Pure water flux L/(m^2•h•psi)	Contact angle
PET non-woven support	104.4 ± 1.7	19300 ± 8900	›400 [20]	39.8 ± 2.7	12360 ± 386	--
Electrospun PAN scaffold	37.3 ± 6.4	220 ± 50	0.78 ± 0.1	79.7	3020 ± 230	57.6 ± 0.2^{o}[20]
Cellulose nanofiber layer	0.24 ± 0.03	~4.3[20]	~0.083	--	~15.3	10.9 ± 0.1^{o}[21]

Table 1: The properties of electrospun PAN nanofibrous scaffold, PET non-woven substrate and cellulose nanofiber barrier layer of cellulose nanofiber membrane.

Cellulose Source	5.4 mmol NaClO/g cellulose		8.7 mmol NaClO/g cellulose	
	-COOH	-CHO	-COOH	-CHO
	(mmol/g cellulose sample)			
Biofloc 96	0.95 ± 0.13	0.34 ± 0.05	1.89 ± 0.06	0.00
Cotton linter ER10	0.98 ± 0.07	0.07 ± 0.04	1.56 ± 0.06	0.05 ± 0.03
Cotton linter UVE	1.00 ± 0.02	0.02 ± 0.01	1.48 ± 0.13	0.06 ± 0.04

Table 2: List of functional group contents in different cellulose sources under two different oxidation conditions: 5.4 and 8.7 mmol NaClO/g cellulose sample.

	Biofloc 96	Cotton linter ER10 DPw 1320	Cotton linter UVE DPw 7350
Pure water flux (Lm^2h/psi)	11.3 ± 3.3	7.8 ± 4.8	10.1 ± 8.5
Rejection rate (2000K Dextran)	70 ± 6%	47 ± 7%	42 ± 4%

Table 3: Summary of filtration performance of cellulose nanofiber UF membranes based on different cellulose sources

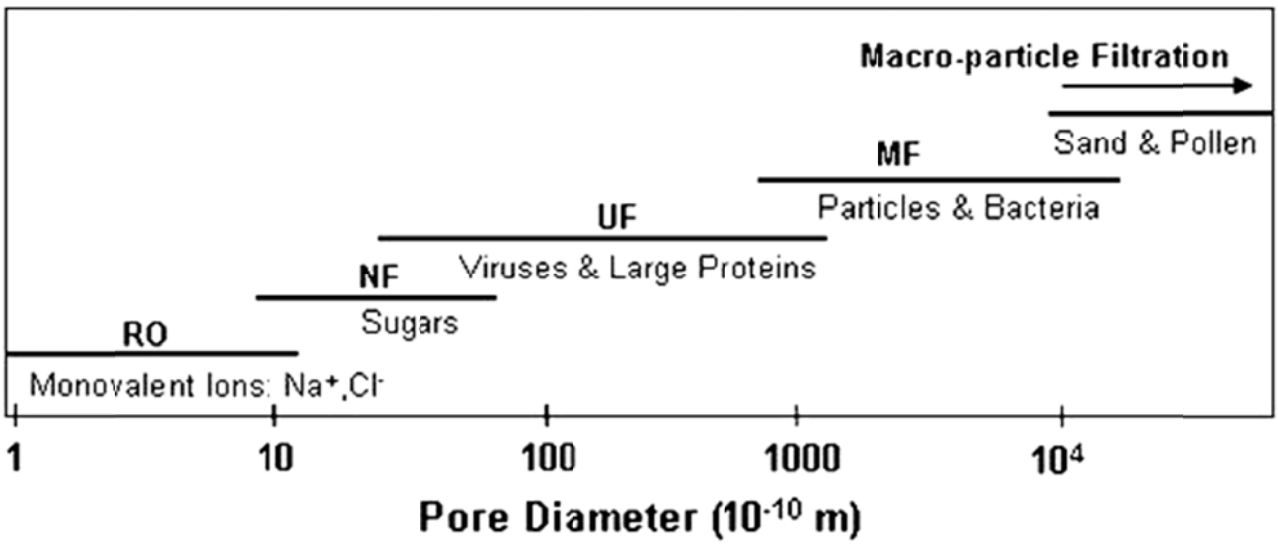

Figure 1: Classification of water filtration based on pore diameter size

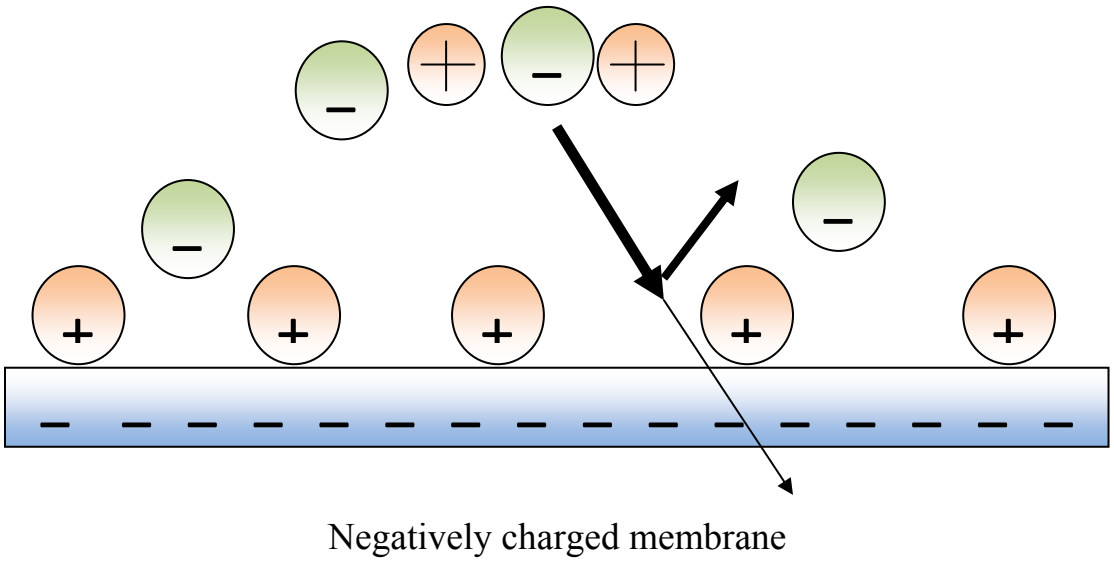

Figure 2: The schematic of the Donnan effect on a negatively charged membrane

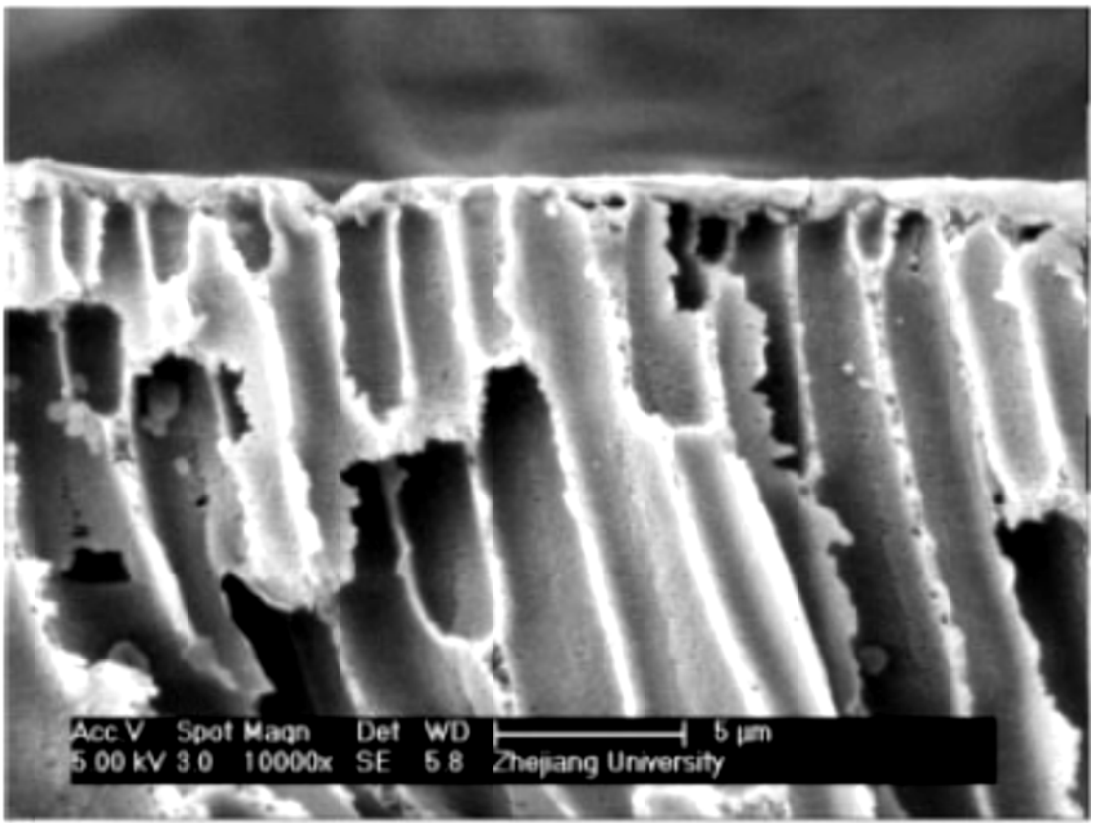

Figure 3: The cross-section SEM image of a polysulfone (PS) membrane

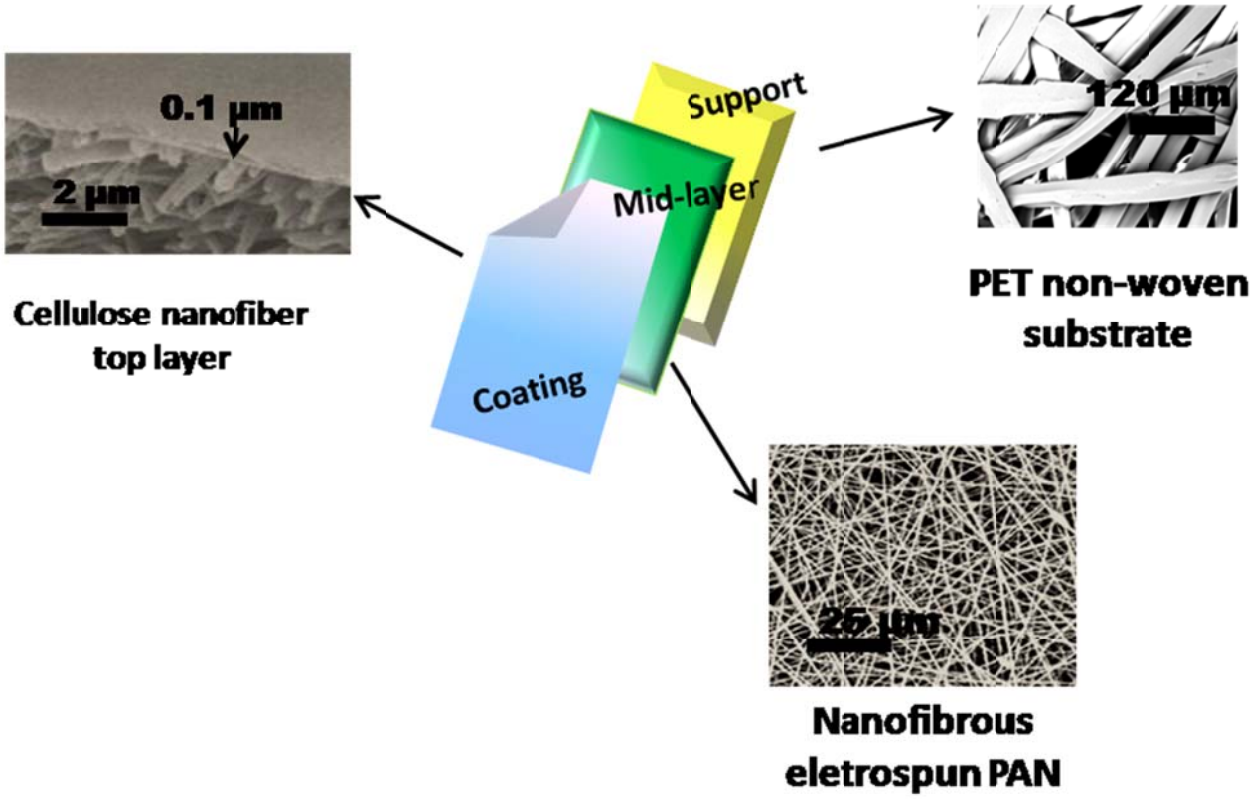

Figure 4: The schematic diagram of the novel structure of cellulose nanofiber membrane

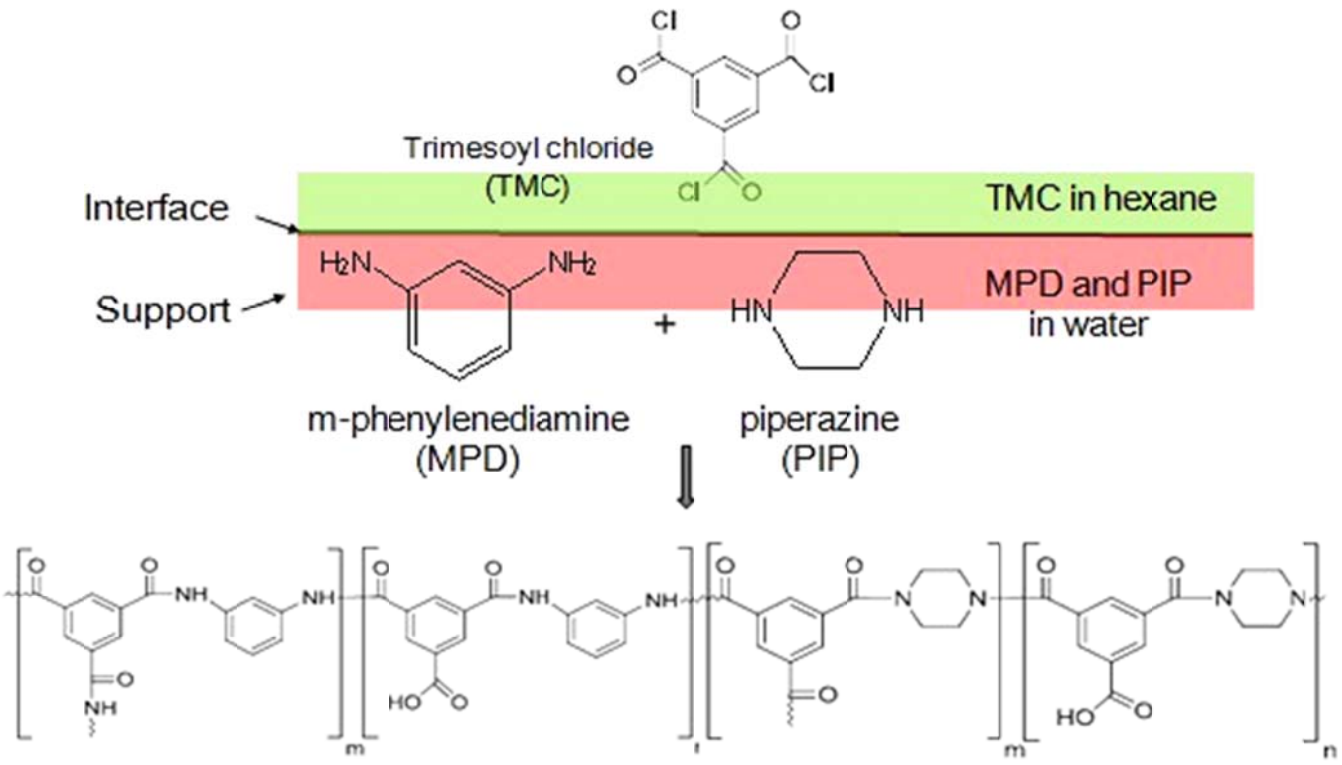

Figure 5: The schematic diagram of the formation of polyamide barrier layer by interfacial polymerization between MPD, PIP and TMC.

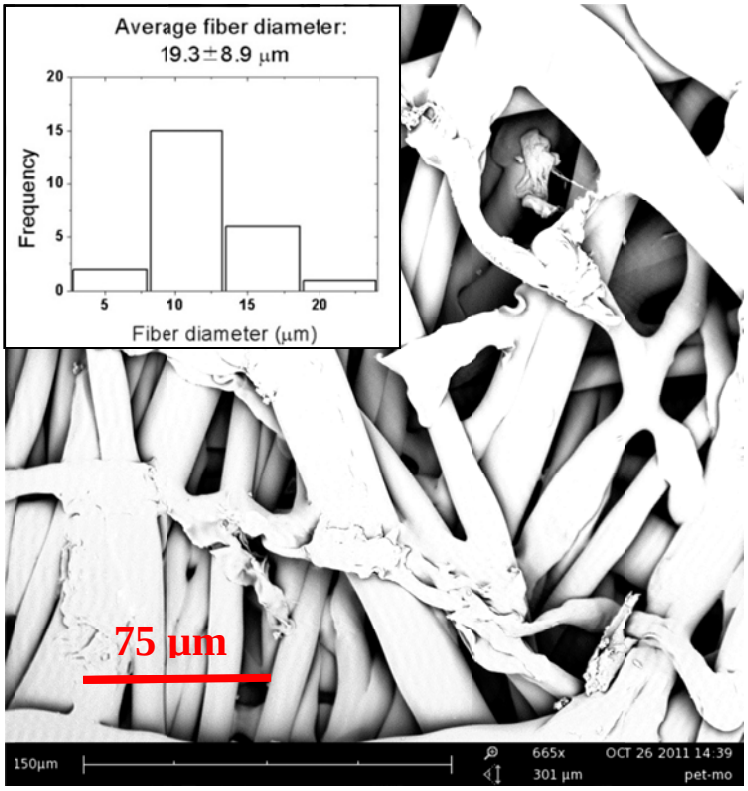

Figure 6: The top view SEM of the PET non-woven support and its fiber diameter distribution

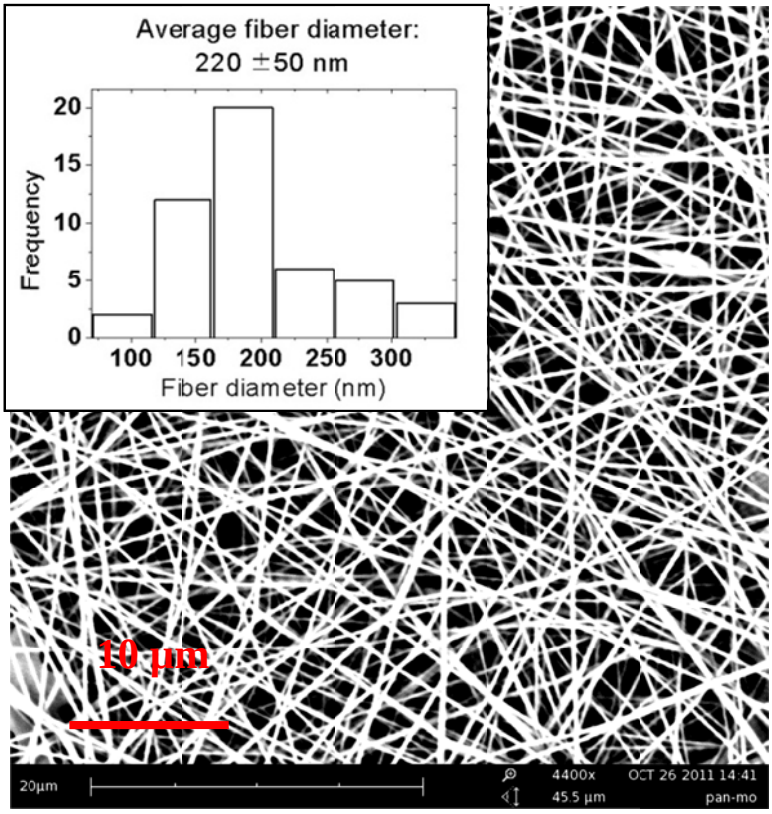

Figure 7: The top view SEM image of the PAN nanofibrous scaffold and its fiber diameter distribution

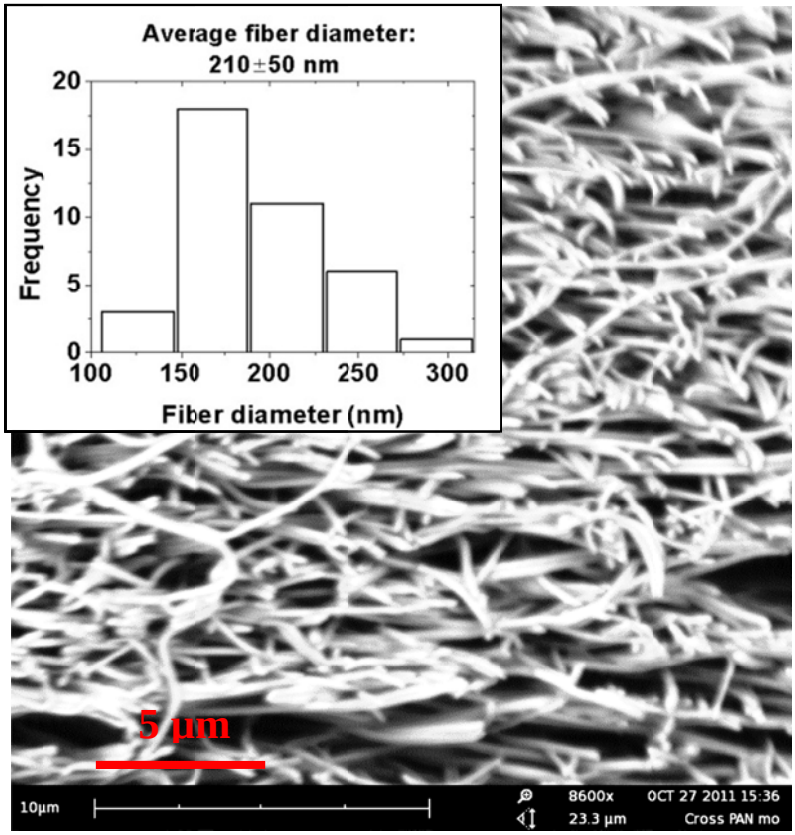

Figure 8: The cross-section view SEM image of the PAN nanofibrous scaffold and its fiber diameter distribution

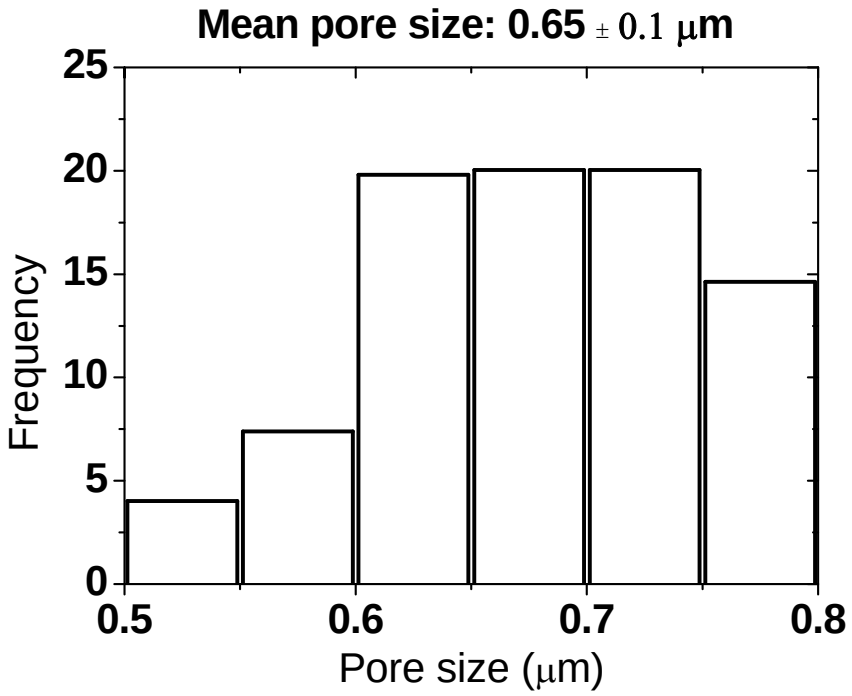

Figure 9: Pore size distribution of PAN nanofibrous scaffold.

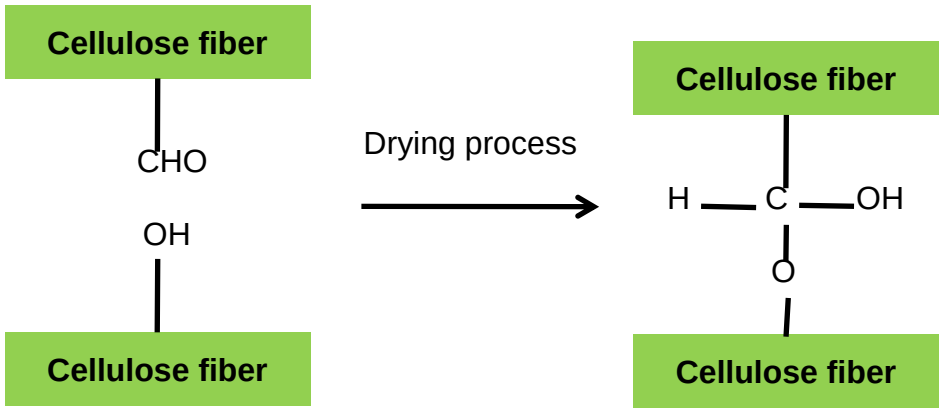

Figure 10: The thermal crosslinking reaction between C6 hydroxyl group and aldehyde group

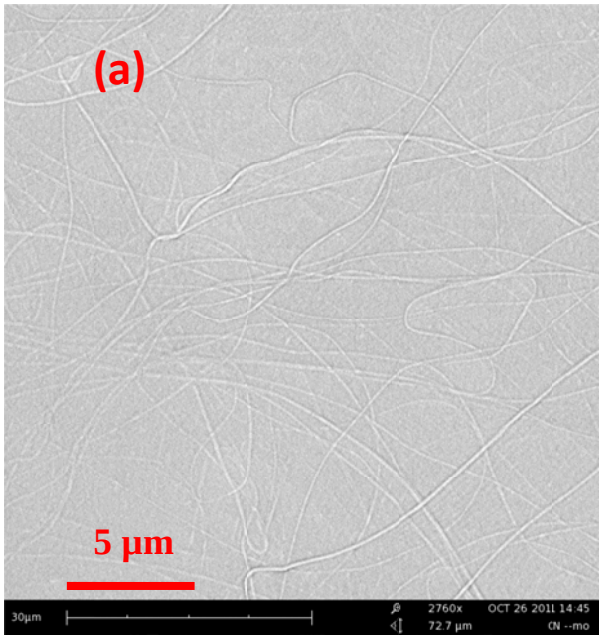

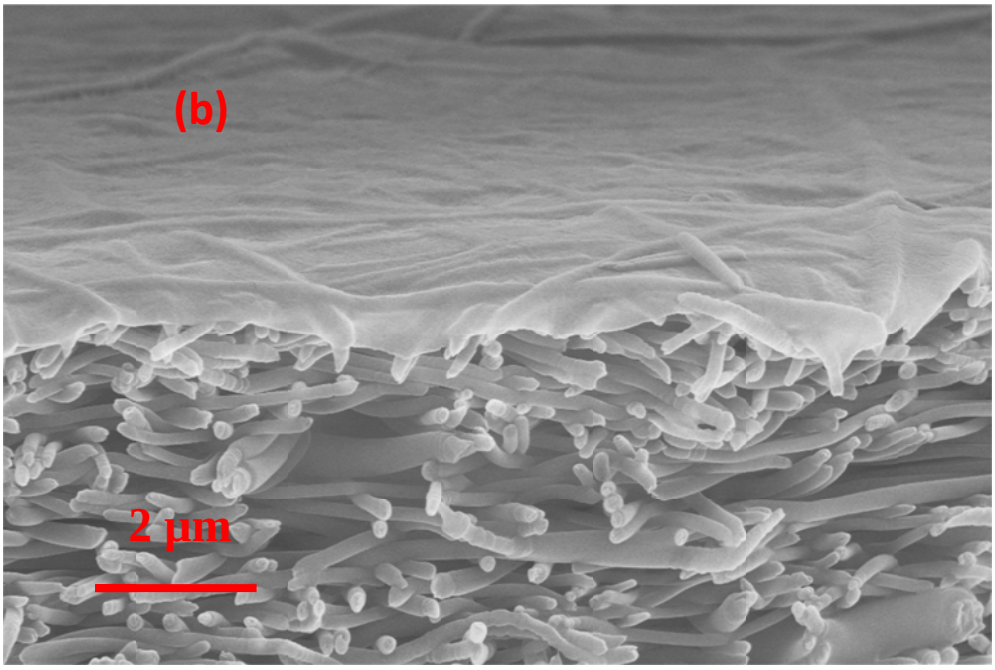

Figure 11: (a) The top and (b) cross-section view SEM images of cellulose nanofiber layer

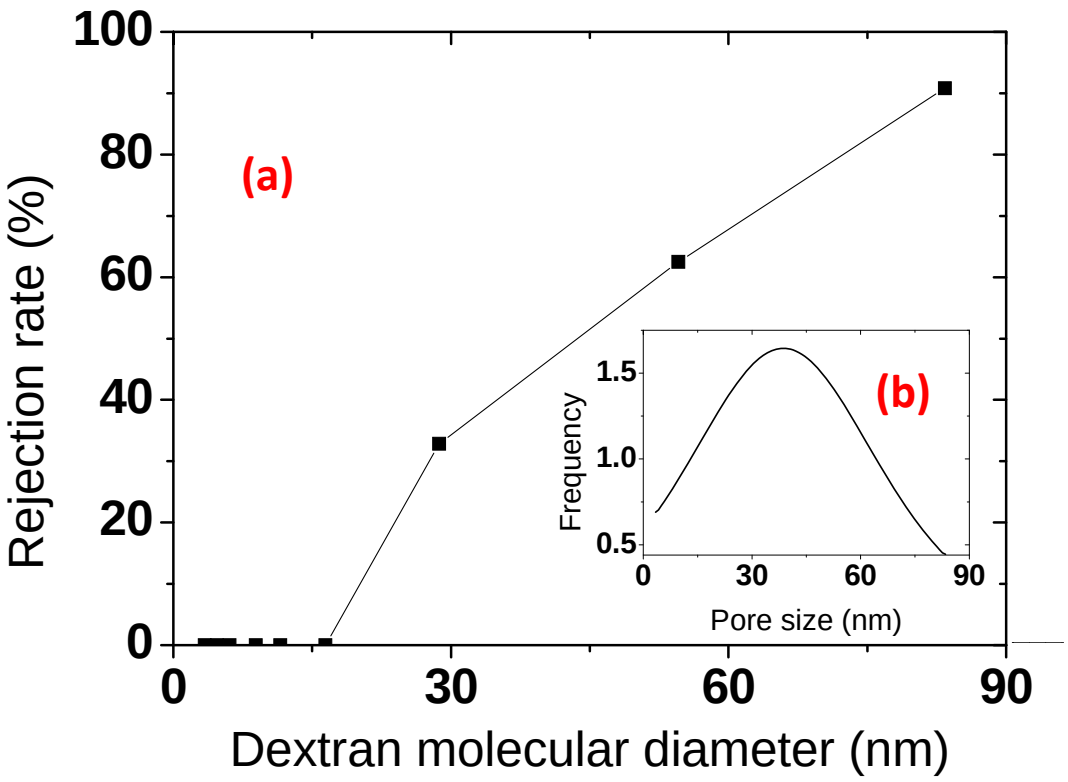

Figure 12: (a) MWCO test result of cellulose nanofiber membrane and (b) its pore size distribution

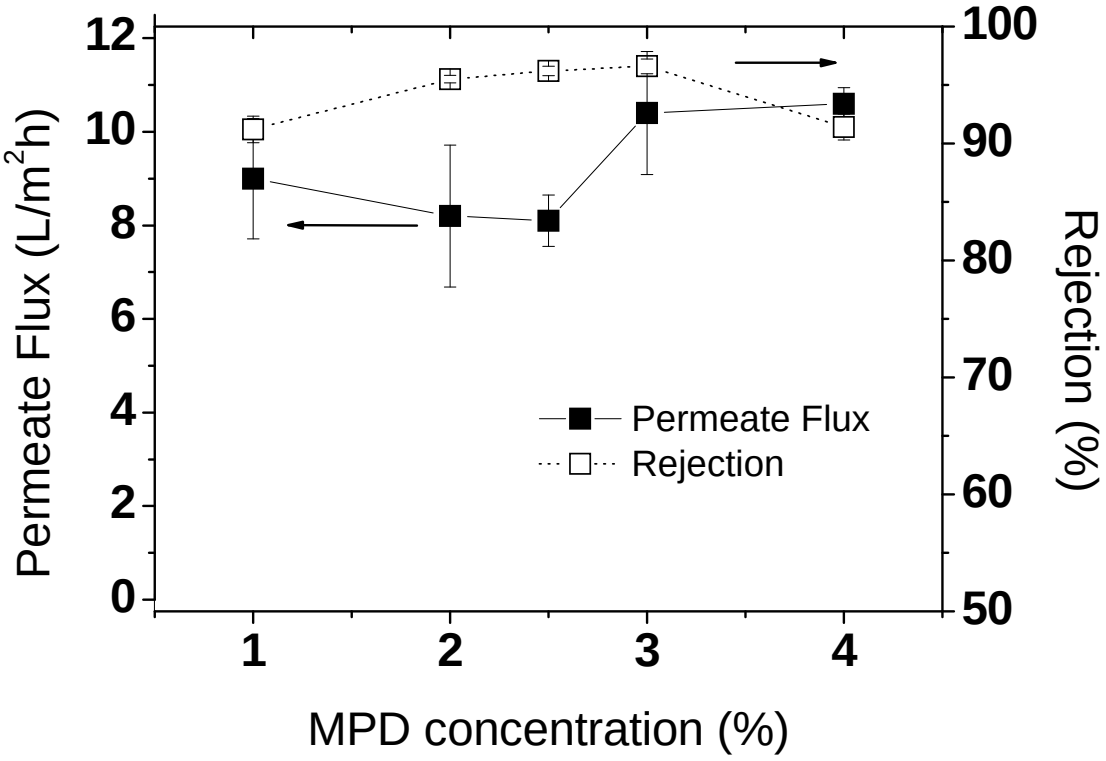

Figure 13: The effect of MPD concentration change on the RO filtration performance

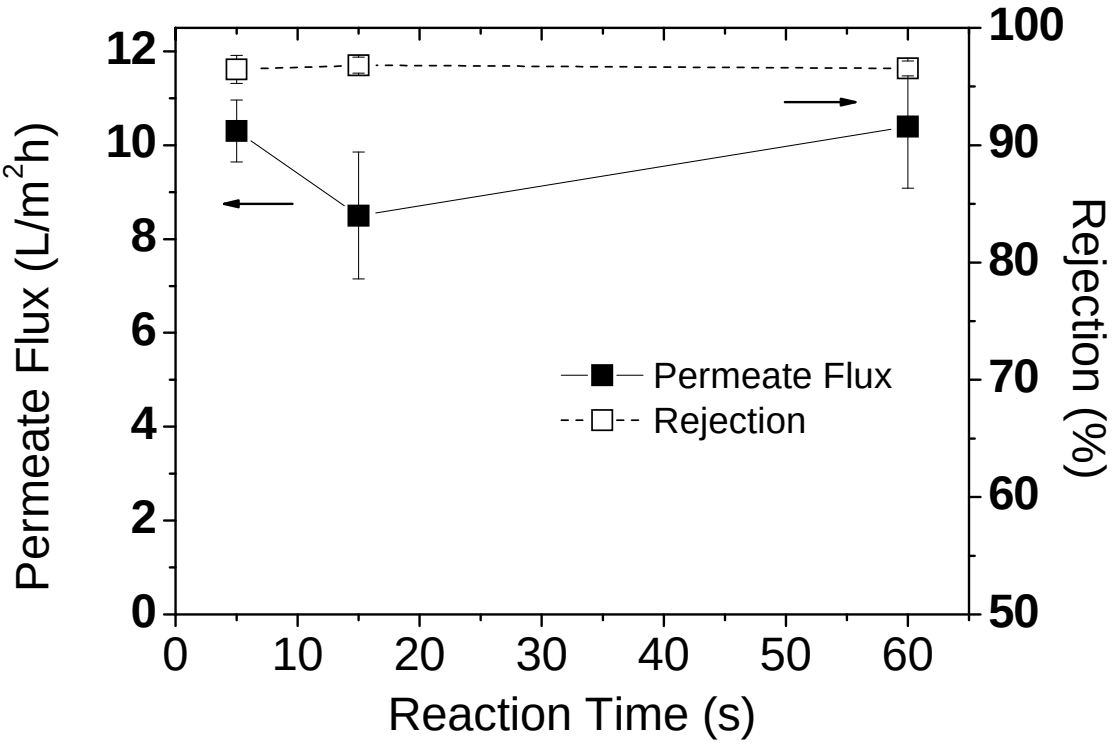

Figure 14: The effect of reaction time on filtration performance

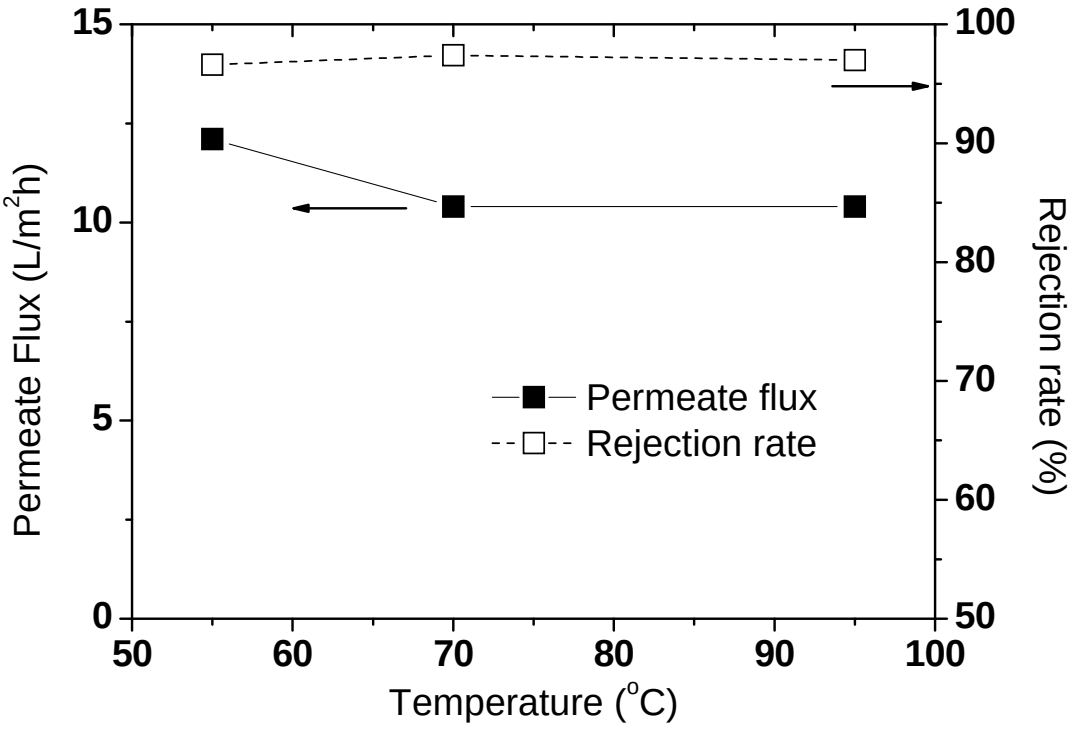

Figure 15: The effect of curing temperature on the filtration performance

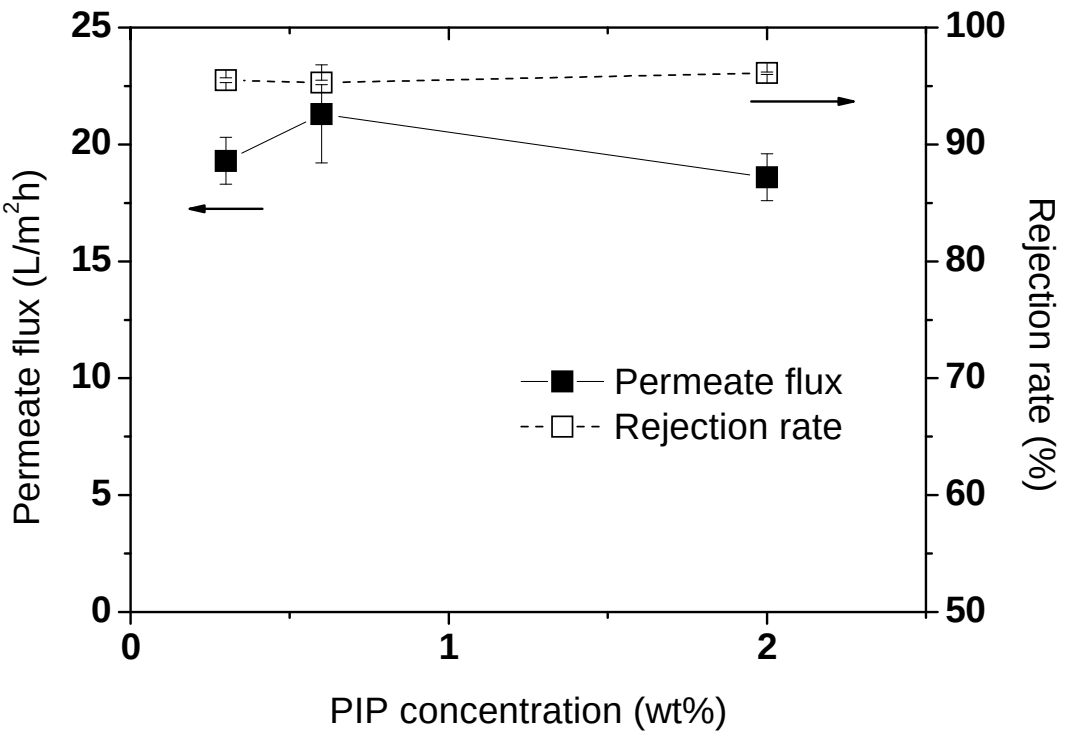

Figure 16: The filtration performance of different PIP concentrations at 3% MPD

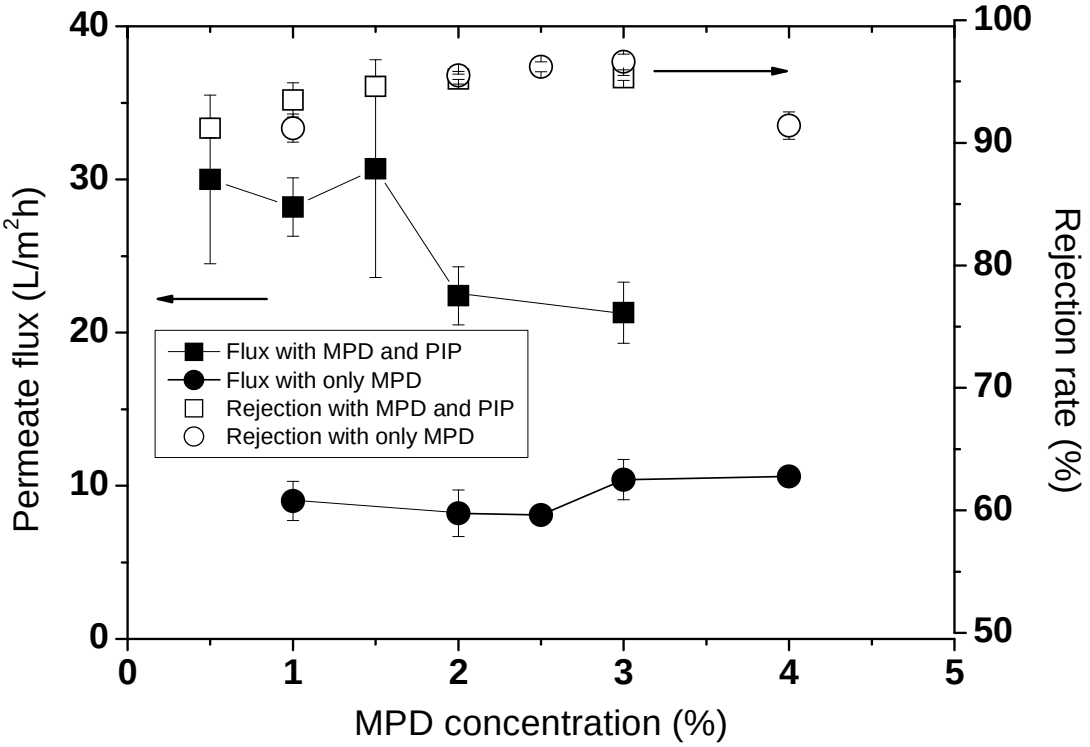

Figure 17: The filtration performance of different MPD concentrations at 0.5% PIP and comparison with that of only different MPD concentrations

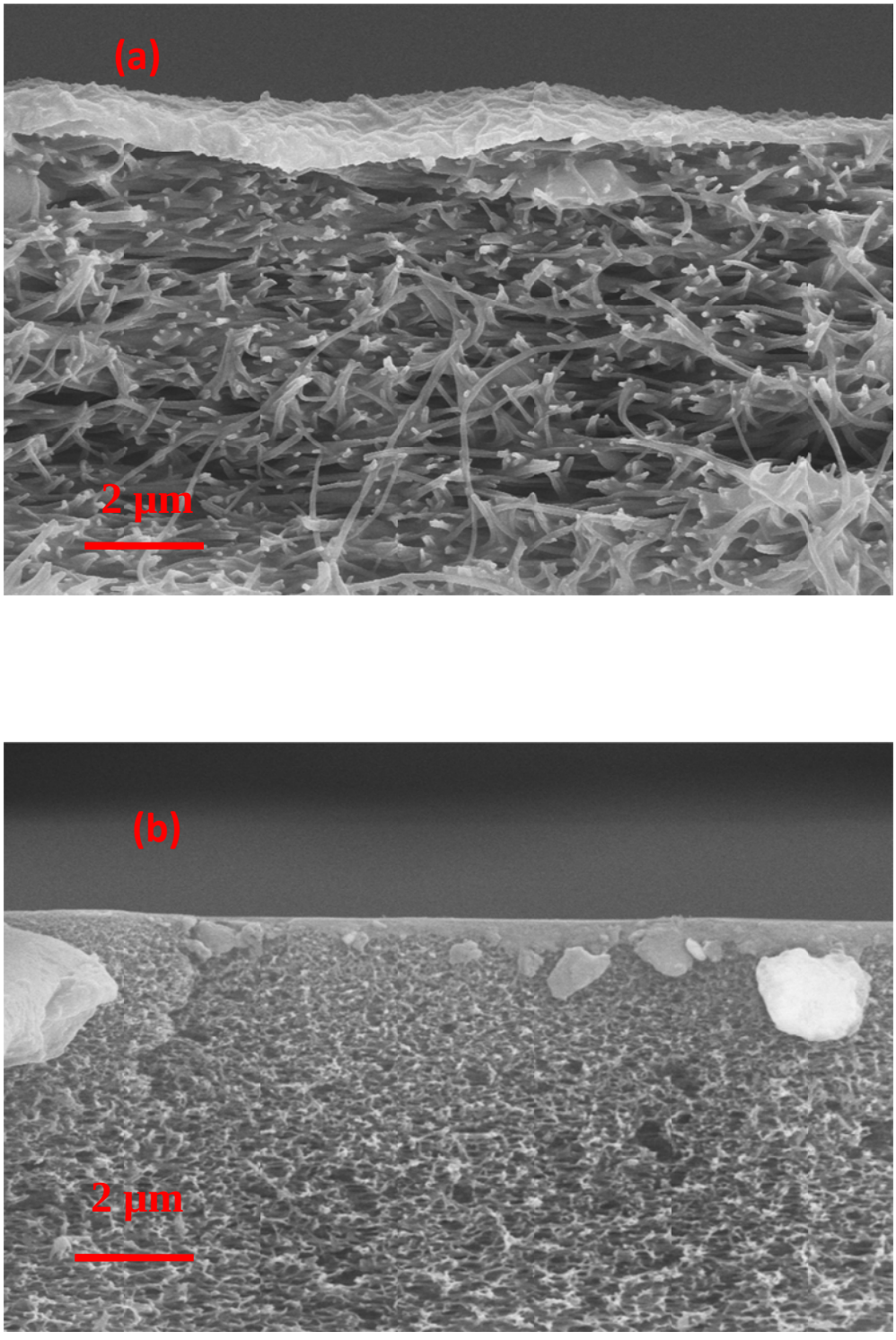

Figure 18: Cross-section SEM images of (a) thin film nanocomposite membrane and (b) Dow filmtec XLE-440

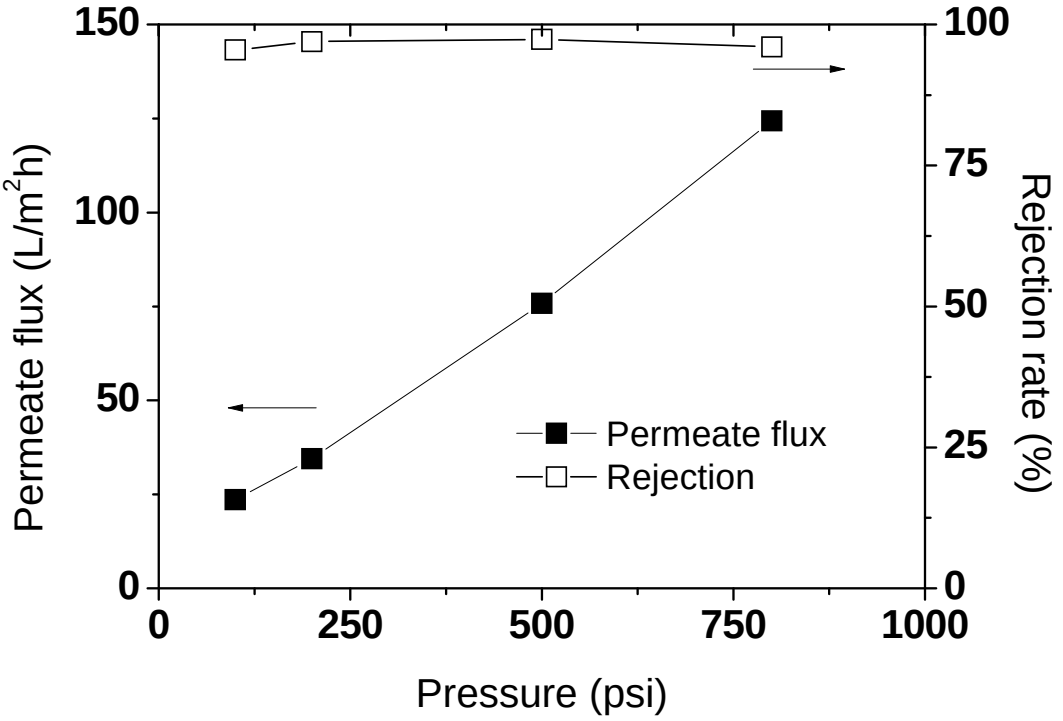

Figure 19: RO filtration performance test of RO membrane with CN substrate under various applied pressure (100~800 psi)